J Paleolimnol (2016) 55:67–82
DOI 10.1007/s10933-015-9863-1

ORIGINAL PAPER

Biogeochemical evidence for freshwater periods during the Last Glacial Maximum recorded in lake sediments from Nam Co, south-central Tibetan Plateau

Roman Witt · Franziska Günther · Stefan Lauterbach · Thomas Kasper · Roland Mäusbacher · Tandong Yao · Gerd Gleixner

Received: 30 July 2014 / Accepted: 6 October 2015 / Published online: 6 November 2015

Abstract Improved knowledge of deglaciation processes during the termination of the Last Glacial Maximum on the Tibetan Plateau can provide important information for understanding deglaciations in climate-sensitive high-altitude ecosystems. Little, however, is known about this time interval because most lacustrine sediment records from the Tibetan Plateau are younger than 19,000 years. This study focused on a lake sediment record from Nam Co, south-central Tibetan Plateau, covering the interval from ~23.7 to 20.9 cal ka BP. We analysed the distribution and compound-specific hydrogen isotope composition (δD) of sedimentary *n*-alkanes, as well as the bulk sediment TOC, TN, $\delta^{13}C_{org}$ and $\delta^{15}N$ composition, to infer lake system development. Pronounced changes in environmental conditions between ~21.6 and 21.1 cal ka BP, as well as between 23.1 and 22.5 cal ka BP (Greenland Interstadial 2), were inferred from increased aquatic *n*-alkane amounts and decreased δD_{n-C23} values within these time intervals, respectively. Freshwater inputs, which most likely resulted from enhanced glacier melting, caused these changes. Our results suggest that mountain glacier retreat on the Tibetan Plateau started earlier than previously assumed. The required energy for thawing was probably provided by temperature changes caused by reorganization of atmospheric circulation, which has also been recorded in Greenland ice records.

Keywords Last Glacial Maximum · Deglaciation · Lake sediments · Compound-specific hydrogen isotopes · *n*-Alkanes · Tibetan Plateau

Electronic supplementary material The online version of this article (doi:10.1007/s10933-015-9863-1) contains supplementary material, which is available to authorized users.

R. Witt · F. Günther · G. Gleixner (✉)
Max Planck Institute for Biogeochemistry, Hans–Knöll–Str. 10, 07745 Jena, Germany
e-mail: gerd.gleixner@bgc-jena.mpg.de

S. Lauterbach
GFZ German Research Centre for Geosciences, Section 5.2 – Climate Dynamics and Landscape Evolution, 14473 Potsdam, Germany

T. Kasper · R. Mäusbacher
Friedrich Schiller University, 07747 Jena, Germany

T. Yao
TEL Institute of Tibetan Plateau Research, Chinese Academy of Sciences, Beijing 100085, China

Introduction

Global climate change and associated temperature increase have particularly strong effects on high-altitude freshwater resources, through glacier melting, increased evaporation and loss of water-storage capacity. In this regard, the Tibetan Plateau, with the world's third largest amount of glaciers and numerous lakes, represents a key region of interest, especially because it is the main freshwater source area for millions of people in Asia. Nam Co, the second largest Tibetan lake, which is located close to a large glaciated area on the south-central Tibetan Plateau, has already shown a clear response to current warming (Bolch et al. 2010). Hence, investigating past, large-scale climate changes in the Nam Co region, e.g. the Last Glacial Maximum (LGM), can contribute to the understanding of developmental stages during deglaciation, and thus shed light on environmental changes that the region is experiencing today and under future warming.

Because of the more equatorial position of the Intertropical Convergence Zone during the LGM (Chabangborn et al. 2014; Günther et al. 2015), the Indian Ocean Summer Monsoon (IOSM), which today provides moist air masses to the Tibetan Plateau, was much weaker (Barrows and Juggins 2005). As a consequence, the winter monsoon in the interior of the Tibetan Plateau, which is related to the interplay between the Siberian High and the mid-latitude Westerlies, is assumed to have been stronger because of the weaker thermal contrast between the Asian continent and the ocean (Shi 2002). The resulting dominance of colder and dryer air masses may have caused a decrease in annual precipitation, from 1000 to 200 mm, which forced the expansion of continental glaciers under extreme cold during the LGM, resulting in glacier extent on the Tibetan Plateau 15 times larger than today (Shi 2002). Globally, the LGM was characterized by greater extent of ice sheets (Mix et al. 2001), lower sea levels and air temperatures 6–9 °C lower than today (Lambeck et al. 2002; Shi 2002). Although the LGM is generally defined as occurring from 26 to 19 ka BP (Clark et al. 2009), the related maximum extent of glaciated areas reveals large spatial and temporal differences (Hughes et al. 2013). The Greenland ice core records, i.e. the most investigated climate archives, show evidence for rapid climate events within the LGM (Lowe et al. 2008). Deglaciation on the Tibetan Plateau, especially in the Nam Co region, is thought to have occurred between 18 and 16 ka BP, similar to the timing of deglaciation in the Southern Hemisphere and thus later than in other regions (Clark et al. 2009). The precise timing of deglaciation in this area, as well as local environmental changes during this period, are still a matter of debate (Clark et al. 2009; Hou et al. 2012).

Although the distribution of *n*-alkanes and their stable hydrogen isotope composition (δD) have been used successfully to reconstruct Holocene environmental and climatic changes (e.g. humidity and temperature) at Nam Co (Xia et al. 2008; Mügler et al. 2010), such analyses have not yet been applied to LGM sediment records. Sediment *n*-alkane distribution reflects sources of organic matter input, and the *n*-alkane isotopic composition reflects the signal of source water, which can thus be used to distinguish between meltwater and precipitation water (Aichner et al. 2010b; Günther et al. 2013; Hu et al. 2014).

In this study, analysis of the distribution and δD composition of sedimentary *n*-alkanes, as well as bulk sediment geochemical analyses ($\delta^{13}C_{org}$, $\delta^{15}N$, TOC, TN), were applied to sediments of the late LGM (23.7–20.9 cal ka BP) from Nam Co. These investigations aimed to characterize environmental changes during this time interval at Nam Co and improve our understanding of climate and environmental changes on the broader Tibetan Plateau. Our goal was to improve understanding of regional climate characteristics during the transition from full glacial to deglaciation conditions in this climatically sensitive region. Specifically, we focused on (1) inferring lake development and changes in climate and productivity during this period, and (2) clarifying whether continuous ice cover persisted during this interval and, if not, which processes provided thawing energy to the lake system.

Study area

Lake Nam Co is located in the south-central part of the Tibetan Plateau (30°30′–30°56′N, 90°16′–91°03′E) at an elevation of 4722 m a.s.l. (Lin et al. 2008; Schütt et al. 2010) (Fig. 1). The lake is approximately 70 × 30 km, with a surface area ~2015 km^2 in 2004 (Zhu et al. 2010), a maximum water depth of 99 m (Daut et al. 2010) and a catchment area of about 10,600 km^2 (Wang et al. 2011). Recent climate at Nam Co can be characterized as semi–arid to semi-humid, continental (Mügler et al. 2010), with a mean annual evaporation of 790 mm for the lake surface and 320 mm for the catchment (Li et al. 2008). Most local precipitation is delivered by the IOSM during summer, whereas during winter, cold and dry air masses of the Westerlies and the Siberian High prevail (Chen et al. 2012). Mean annual precipitation varies between 300 and 500 mm (Zhu et al. 2010) and the mean annual air temperature is −1 °C (Schütt et al. 2010). Because the Nam Co basin is closed (Schütt et al. 2010), water

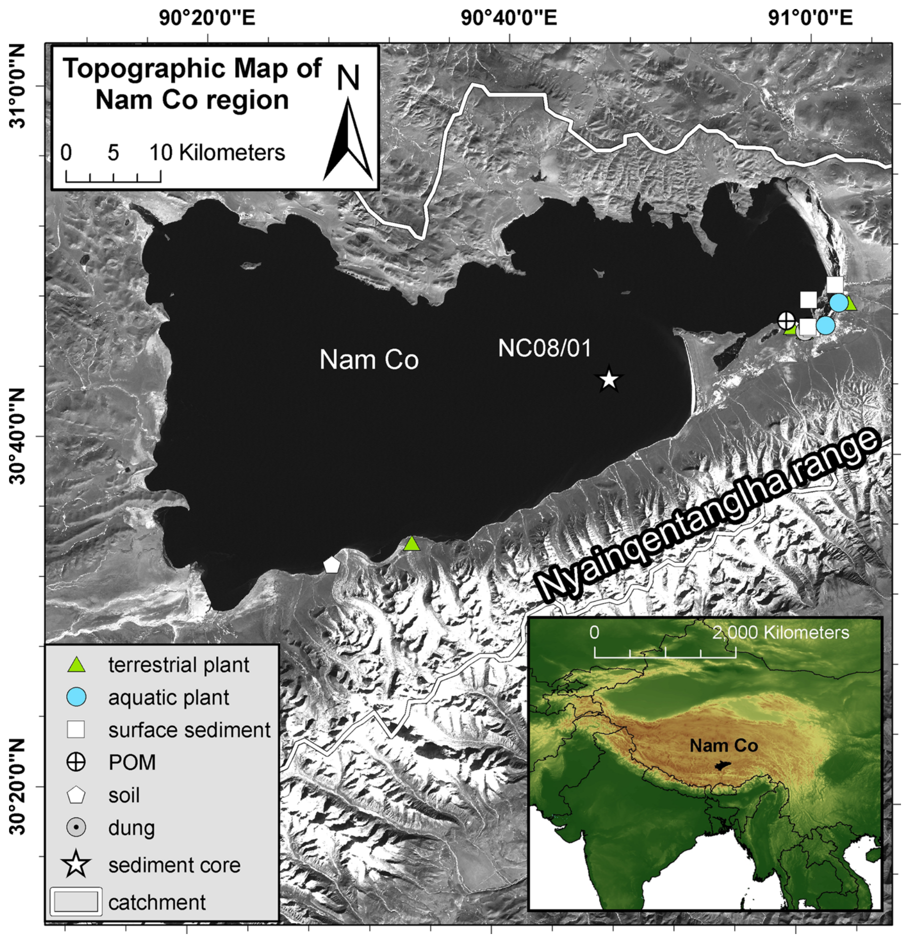

Fig. 1 Location map of Nam Co, south-central Tibet (satellite image obtained from www.landsat.org). The location of sediment core NC 08/01 in the south-eastern basin is marked by a star. Locations of plant, surface sediment, soil and particulate organic matter (POM) samples are marked by *symbols* explained in the legend. Nam Co catchment location in Asia is marked in *black*

balance is controlled mainly by evaporation, precipitation and inflow, but is also influenced, negatively, by seepage of lake water into groundwater (Zhou et al. 2013). Positive water balance today is caused by enhanced input of glacial meltwater from the Nyainqentanglha Mountain Range south of Nam Co, which is a consequence of recently rising temperature (Liu et al. 2010). Vegetation within the catchment is adapted to high–altitude climate conditions and is dominated by alpine meadow and steppe grasses such as *Kobresia* sp., *Stipa* sp., *Artemisia* sp., *Oxytropis* sp., *Morina* sp. and *Carex* sp. (Mügler et al. 2008).

Materials and methods

Field sampling

In 2008, a 10.4-m-long composite sediment core (NC 08/01) was recovered from the south-eastern basin of Nam Co (30°44′14.7″N, 90°47′25.2″E), in 93 m of water (Fig. 1), using a piston corer with a diameter of 90 mm (UWITEC, Mondsee, Austria). This study focused on the lowermost part of the sediment core, 10.38–6.60 m composite depth. This core section was sampled at 5–cm intervals, with ~12 g dry sediment for each sample. Additionally, surface sediment samples were taken in 2009 using an HTH gravity corer with a 6.6-cm internal diameter (Pylonex, Luneå, Sweden). The uppermost 1 cm was sampled from these cores. All samples were freeze-dried (P25, Piatkowski, Munich, Germany) and homogenized for further analyses.

Terrestrial plants (e.g. *Carex*, *Kobresia*, *Stipa*, *Leontopodium*, *Potentilla* and *Dasiphora parvifolia*) were collected from the eastern/southern Nam Co catchment and submerged macrophytes (*Potamogeton*) were taken from 2 to 5 m water depth in the eastern Nam Co basin in 2009. Each plant sample consisted of several individuals. In addition, dung from different herbivores was collected, representing the digested residue of plant matter. Catchment soil samples were taken from two depth intervals (0–5 and 5–10 cm) and sieved with 2-mm mesh. All soil, plant and dung samples were air–dried in the field and transported in paper bags. Particulate organic matter (POM) was filtered from a lake water depth of 15 m using a filtration system with a glass fibre filter of 1 µm pore size to trap fine particles, and pre-filters of 50 and 10 µm to collect coarser particles.

Chronology of Nam Co sediment core NC 08/01

The chronology of the complete NC 08/01 sediment core is based on 24 AMS ^{14}C ages (Beta Analytic, Miami, USA) obtained from bulk sediment samples (Doberschütz et al. 2014; Kasper et al. 2015) using calibrated median ages of the 2σ distribution provided by OxCal 4.1.7 (Bronk Ramsey 1995). The investigated core section between 10.38 and 6.60 m includes 5 AMS ^{14}C ages [Fig. 2; Electronic Supplementary Material (ESM) Table 1] (Kasper et al. 2015). A reservoir effect of 1420 ^{14}C years was inferred from the age of the core sediment-water interface and was subtracted from all radiocarbon ages prior to calibration (Doberschütz et al. 2014). The interval investigated in this study covers a time span of 2.8 ka, between 23.7 and 20.9 cal ka BP. The mean sediment accumulation rate (SAR) in this section of the sediment record is 1.7 mm a^{-1}.

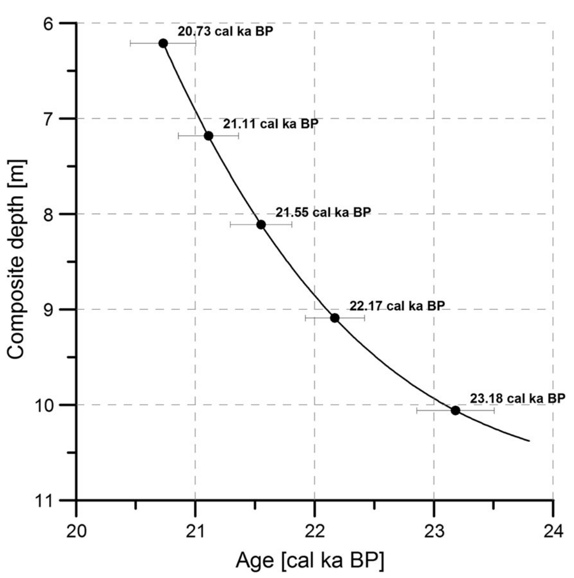

Fig. 2 Chronology of Nam Co sediment core NC 08/01 for the investigated interval, as established from the calibrated median ages of five radiocarbon dates on bulk sediment samples (Kasper et al. 2015). *Error bars* represent the 2σ uncertainty range

Measurement of sediment $\delta^{13}C_{org}$, $\delta^{15}N$, TOC and TN

For geochemical analyses, homogenized aliquots of dry sediment were weighed in tin capsules (~4 mg for C, ~80 mg for N). Inorganic carbon was removed by adding H_2SO_3 stepwise until 120 µl was added (Steinbeiss et al. 2008), prior to measuring the content of total organic carbon (TOC) and the stable carbon isotope composition ($\delta^{13}C_{org}$) of the organic fraction. TOC and $\delta^{13}C_{org}$, as well as the total nitrogen content (TN) and the stable nitrogen isotope composition ($\delta^{15}N$), were determined in separate runs with a coupled EA–IRMS system (EA: NA 1100 CN–EA, CE Instruments, Milan, Italy; IRMS: Delta C with Delta^{Plus} ion source, Finnigan MAT, Bremen, Germany). Each sample was measured in duplicate to verify sample homogeneity (analytical precision: $\delta^{13}C_{org} = \pm 0.12$ ‰; $\delta^{15}N = \pm 0.12$ ‰). Working standards were acetanilide ($\delta^{13}C = -29.8$ ‰, $\delta^{15}N = -1.5$ ‰) and caffeine ($\delta^{13}C = -40.2$ ‰, $\delta^{15}N = -15.5$ ‰), calibrated against international standards IAEA-N1 and NBS-22. The $\delta^{13}C$ and $\delta^{15}N$ compositions are reported in the conventional δ-notation relative to the Vienna Pee Dee Belemnite (V-PDB) and atmospheric (AIR) nitrogen standards (Werner and Brand 2001).

Analysis of sedimentary and plant *n*-alkanes

Lipid extractions were performed on 6 g of dry core sediment and 2 g of dry surface sediment, plant material (all plant parts were used), dung and soil, using an accelerated solvent extractor (ASE 200, DIONEX Corp., Sunnyvale, USA). The ASE was operated at 100 °C and 138 bar for 15 min in 2 cycles using a 9:1 (v/v) solvent mixture of dichloromethane and methanol. HCl–activated copper (15 % HCl) was added to remove elemental sulphur. The total lipid extract was then separated using solid phase extraction on silica gel (0.040–0.063 mm mesh; Merck, Darmstadt, Germany) according to Sachse et al. (2006). The *n*-alkane (aliphatic) fraction was eluted with 80 ml *n*-hexane.

Identification and quantification of *n*-alkanes from the sediment core samples were accomplished using a GC–FID system (TRACE GC 2000, CE Instruments, Thermo Quest, Rodano, Italy) with a DB-1MS column (30 m length, 0.25 mm ID, 0.25 μm film thickness; Agilent Technologies, Santa Clara, USA) by comparing peak areas and retention times with an external *n*-alkane standard mixture (n-C_{10} to n-C_{34}). The PTV-injector was operated in splitless mode with an initial temperature of 45 °C for 0.1 min and then heated to 300 °C at 14.5 °C s^{-1} for 3 min. The temperature of the GC oven was held at 90 °C for 1 min, raised to 300 °C at 10 °C min^{-1}, kept constant for 9 min and finally increased at 30 °C min^{-1} to 335 °C and held there for 3 min. Helium was used as a carrier gas at a constant flow of 2 ml min^{-1}. The FID was operated at constant temperature of 300 °C with gas flows of 40, 45 and 450 ml min^{-1} for synthetic air, hydrogen and nitrogen, respectively.

The *n*-alkane concentrations of recent plant, soil, dung and sediment samples were measured in a GC–FID system (HP 6890, Agilent Technologies, Santa Clara, USA) with an Agilent 19091B-115 column (50 m length, 0.32 mm ID, 0.52 μm film thickness, Agilent Technologies, Santa Clara, USA). The injector was operated in split mode with a ratio of 10:1 and a constant temperature of 280 °C. The oven programme started at 80 °C and was kept constant for 1 min before increasing at 10 °C min^{-1} to 300 °C. After 11 min, the oven heated at 30 °C min^{-1} to 330 °C and was kept constant for 5 min. Each sample was measured in triplicate. Results are expressed as ng g^{-1} dry weight.

To discriminate between the input of fresh and digested allochthonous plant material, the Carbon Preference Index (CPI) for n-C_{17} to n-C_{31}, which expresses the ratio of *n*-alkanes with an odd number of carbon atoms relative to those with an even number, was calculated according to:

$$\mathrm{CPI}_{17-31} = 0.5 \times \left(\left(\sum\nolimits_{\mathrm{odd}} \mathrm{C}_{15-29}\right) \Big/ \left(\sum\nolimits_{\mathrm{even}} \mathrm{C}_{16-30}\right)\right) + \left(\left(\sum\nolimits_{\mathrm{odd}} \mathrm{C}_{17-31}\right) \Big/ \left(\sum\nolimits_{\mathrm{even}} \mathrm{C}_{16-30}\right)\right) \tag{1}$$

The average chain length (ACL) was calculated according to:

$$\mathrm{ACL}_{17-31} = \sum (\mathrm{C}_n \times n) \Big/ \sum \mathrm{C}_n. \tag{2}$$

Cluster analysis of the sedimentary *n*-alkane distribution was performed with the PASW statistics 18 software, using K-means clustering. Different sources of lacustrine *n*-alkanes were visualized by principal component analysis (PCA) using SigmaPlot 10 software.

Measurement of δD of *n*-alkanes

Stable hydrogen isotope ratios (δD) were analysed using a coupled GC–IRMS system. Because of very low *n*-alkane concentrations (<250 ng g^{-1}), 3–4 sediment samples had to be pooled together. According to the age-depth model, this pooling results in mean δD values spreading over a range of ~80 years in the younger section to ~200 years in the bottom section. The combined samples were injected into a GC system (HP5890 Series II, Agilent Technologies, Böblingen, Germany) equipped with a BP1 column (60 m, 0.32 mm ID, 0.50 μm film thickness; SGE GmbH, Darmstadt, Germany). The injector was operated at a constant temperature of 280 °C in splitless mode. The oven was maintained for 1 min at 60 °C, heated at 10 °C min^{-1} to 300 °C and was kept constant for 28.5 min. The final ramp heated at 20 °C min^{-1} to 340 °C and was kept constant for 3 min. The column flow was constant at 2 ml min^{-1}. Five percent of the gas flow was transferred to an ion trap mass spectrometer (GCQ Thermo Electron, San Jose, USA) to identify mass fragments and 95 % went to an isotope ratio mass spectrometer (Delta^{plus} XL, Finnigan MAT, Bremen, Germany). The δD composition was determined three times for each sample and reported in conventional δ-notation relative to the Vienna Standard Mean Ocean Water (VSMOW). A general offset calculation was accomplished using H_2 reference gas with known isotopic composition and correcting measured δD values from a standard mixture containing several *n*-alkanes (n-C_{10} to n-C_{34}). Outliers were eliminated using Peirce's criterion. The mean standard deviation for all standard triplicates was 5.2 ‰, consequently no drift correction was applied. The H_3^+ factor was determined on a daily basis and stayed constant within the analytical error at 11.44 (SD = 0.52; n = 9) during the measurement period.

Polissar et al. (2009) pointed out that for low-concentration Tibetan samples, additional concentration-dependent corrections are necessary. We calibrated our GC-IRMS system using standard mixtures of five concentrations (5–200 ng μl^{-1}). The δD values increased logarithmically (n-C_{23-31}: $R^2 = 0.91$ to 0.99) below a concentration of 100 ng μl^{-1}. As the majority of samples were below this limit, a concentration-dependent correction was applied (Wang et al. 2008; Wang and Sessions 2008). This correction decreased the δD values of small peaks between 2.3 and 4.3 ‰. However, the correction did not change the significance of differences between the data points in the time series.

Results

$\delta^{13}C_{org}$, $\delta^{15}N$, TOC and TN of catchment samples and lake sediments

Soil geochemical values (n = 2) are close to those of lake sediments, with a mean $\delta^{13}C_{org}$ of −24.9 ‰ and TOC/TN ratios of 7.7 ± 0.5 (ESM Fig. 1). Modern terrestrial plant samples (n = 3) reveal clearly higher TOC/TN ratios (21 ± 5), whereas $\delta^{13}C_{org}$ values plot in the same range for soils and sediments (−25 ± 2 ‰). In contrast, samples of the submerged macrophyte *Potamogeton* (n = 2) show highest values for $\delta^{13}C_{org}$ (−6.4 ± 0.6 ‰) and for TOC/TN ratio (28 ± 7). The highest enrichment in ^{15}N (as $\delta^{15}N$) was determined in the NC08/01 sediments (n = 78; 7.8 ± 0.5 ‰), showing a significant difference ($p < 0.05$) from recent aquatic macrophytes (5.1 ± 1.9 ‰), terrestrial plants (4.4 ± 2.3 ‰) and soil samples (2.9 ± 1.2 ‰).

In the lower part of the investigated core Section (10.38–8.75 m, 23.7–22.0 cal ka BP) $\delta^{13}C_{org}$ and $\delta^{15}N$ show no clear trends, with mean values of −26.4 ± 0.7 ‰ and 8 ± 0.4 ‰, respectively (Fig. 3a, b). Within the upper unit (8.75–6.60 m, 22.0–20.9 cal ka BP) $\delta^{13}C_{org}$ values increase from −27.5 to −24 ‰ and $\delta^{15}N$ values reveal a decreasing trend, from 8.6 to 6.6 ‰. The two variables are significantly negatively correlated ($r = -0.63$, $p < 0.01$). The mean content and variability of TOC (0.42 ± 0.05 %) are much higher than those for TN (0.05 ± 0.003 %). Hence, the TOC/TN ratio (7.9 ± 0.8) is mainly influenced by changes in TOC content (Fig. 3c, d, e). The lower unit is characterized by a mean TOC/TN ratio of 7.3 ± 0.6, whereas the upper part of the investigated section shows a higher mean value (8.4 ± 0.7) because of increasing TOC content. Between 22.4 and 22.0 cal ka BP, TOC and TN both reach lowest values, and the mean TOC/TN ratio is relatively low (7 ± 0.5).

Distribution and concentration of *n*-alkanes

Catchment (soils, terrestrial and aquatic plants, dung, POM) and surface sediment samples

The composition of *n*-alkanes in terrestrial plant samples, but also in dung as decomposition products of terrestrial plants and soil biomass, reveals an increasing predominance of long-chain *n*-alkanes n-$C_{29/31}$ (ACL = 29, 29.8 and 29.9, respectively), with a clear odd/even preference (ESM Fig. 2). The odd/even preference is also visible in the aquatic plants, although mid-chain *n*-alkanes n-$C_{23/25}$ (ACL = 23.7) are dominant. This bimodal distribution of long- and mid-chain *n*-alkanes within plant biomass is also reflected in the Nam Co surface sediments (ACL = 25.9), showing the generally high contribution of terrestrial plant material to lacustrine organic matter. POM within the lake water is characterized by an *n*-alkane distribution between n-C_{15} and n-C_{25} (ACL = 21.1), a low CPI (1.5) and therefore no odd/even predominance.

Sediment core NC 08/01

Sediments of core NC 08/01 contain *n*-alkanes n-C_{15} to n-C_{31}, with a mainly bimodal distribution and maximum at n-C_{23} (104 ng g^{-1}), followed by n-C_{25} (82 ng g^{-1}) and n-C_{31} (73 ng g^{-1}) (ESM Figs. 2, 4). Total concentration of *n*-alkanes n-C_{15-31} ranges between 300 and 1700 ng g^{-1}. The mid- and long-chain *n*-alkanes reveal an odd/even preference, whereas *n*-alkanes $<n$-C_{21} have higher even-carbon-number *n*-alkane amounts. The aquatic biomarker n-C_{23} and the terrestrial n-C_{31} show similar concentration variability (mean values = 111 ± 40 ng g^{-1}, 78 ± 39 ng g^{-1}, respectively) compared to the terrestrial biomarker n-C_{29} (mean value = 63 ± 22 ng g^{-1}). n-C_{23} and n-C_{29} show minimum concentrations at ~21.7 cal ka BP, whereas n-C_{31} could not even be detected at ~22.5 cal ka BP. Maximum

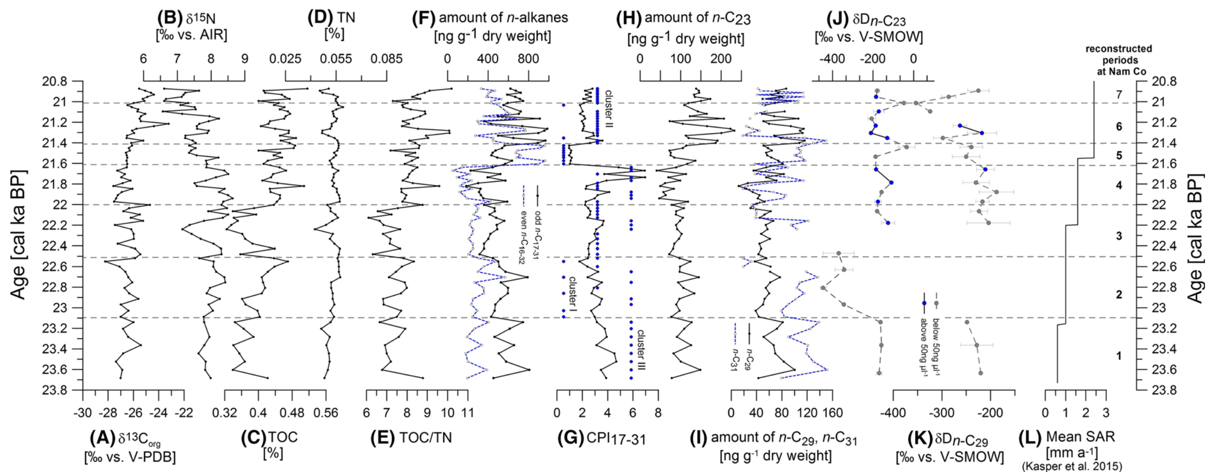

Fig. 3 Climate proxy records for sediment core NC 08/01 between 23.7 and 20.9 cal ka BP. **a** $\delta^{13}C_{org}$ of bulk sediment, **b** $\delta^{15}N$ of bulk sediment, **c** TOC content of bulk sediment, **d** TN content of bulk sediment, **e** TOC/TN ratio, **f** amount of odd-numbered ***n*-al**kanes (n-$C_{17–31}$) and even-numbered ***n*-al**kanes (n-$C_{16–32}$), **g** calculated Carbon Preference Index (CPI) for ***n*-al**kanes n-$C_{17–31}$ (*solid line*) and alkane cluster I–III (*blue dots*), **h** amount of ***n*-al**kane n-C_{23}, **i** amount of ***n*-al**kane n-C_{29} (*solid black line*) and n-C_{31} (*dashed blue line*), **j** δD of n-C_{23} and **k** δD of n-C_{29}, where *grey dots* represent samples below 50 ng μl^{-1} and *blue dots* samples above 50 ng μl^{-1}, **l** mean sediment accumulation rate (Kasper et al. 2015). *Error bars* indicate the standard deviation. (Color figure online)

concentrations appear at 23.6 (n-C_{31}) and ~21.3 cal ka BP (n-C_{23}) (Fig. 3h, i).

A principal component analysis (PCA) of the relative *n*-alkane distribution from sediments of core NC 08/01, as well as surface sediments, terrestrial and aquatic plants, dung, soil and POM, reveals the different sources of lacustrine organic matter (ESM Fig. 3). The *n*-alkane n-C_{29} has a strong positive loading on Axis 1 (57.6 %), whereas short- to mid-chain *n*-alkanes n-$C_{16–25}$ have negative loadings. The terrestrial signal consists of terrestrial plants, dung and soil, with the former controlled mainly by long-chain *n*-alkanes n-C_{29} and soils more strongly controlled by n-C_{31}. Generally, they are clearly distinguished from the aquatic signal, consisting of aquatic plants, surface sediments and POM.

Using the *n*-alkane distribution, the core was separated into three clusters using cluster analysis (ESM Fig. 4). Sediment samples in cluster I (microbial) have no odd/even predominance of *n*-alkane chain length and thus a very low CPI (1.4). This cluster is very characteristic for Periods 2 and 5. Sediments in clusters II and III are dominated by odd mid- and long-chain *n*-alkanes. Whereas samples in cluster II (aquatic) show high abundances of the mid-chain *n*-alkanes n-C_{23} and n-C_{25}, dominance in cluster III (terrestrial) is shifted toward odd carbon numbers $\geq n$-C_{23}, particularly toward n-C_{31}. The CPIs for clusters II and III are 2.3 and 3.3, respectively. The two clusters show no difference in the abundance of short-chain *n*-alkanes $\leq n$-C_{22}. Cluster II is characterized by decreasing abundance with increasing *n*-alkane chain length $>n$-C_{22}, whereas cluster III reveals a shift towards an increasing trend of *n*-alkanes $>n$-C_{29}.

δD values of *n*-alkanes in lake sediments

δD data of the most abundant aquatic *n*-alkane, n-C_{23} (δD_{n-C23}) in the Nam Co LGM sediments, enable division of the profile into three sections, with two recording a mean value of −156 ± 48 ‰, i.e. in the bottom and the upper part (Fig. 3j). In the upper part, two excursions appear, with greater values at ~21.4 and 21 cal ka BP. Nevertheless, such single events should not be over-interpreted, given measurement uncertainties. The other section differs significantly ($p = 0.00$, Tukey HSD) from those above and below, with a low mean value of −376 ± 49 ‰ between 23.1 and 22.4 cal ka BP. A moderate decrease is maintained in the terrestrial n-C_{29} above 22 cal ka BP (−200 to −350 ‰), prior to rapid enrichment in the youngest part of the core (Fig. 3k). Because of low biomarker concentrations, continuous interpretable δD records could not be derived for n-C_{29} for a period of 960 years, from ~23 to 22.2 cal ka BP. A nearly

300-year-long data gap occurred for n-C_{23} between 22.47 and 22.17 cal ka BP.

Identification of lake periods

The investigated core interval can be divided into seven periods (1–7) according to variations in the bulk geochemical data, n-alkane distribution and δD values (Fig. 3). Period 1 (23.7–23.1 cal ka BP) shows high fluctuations of odd- and even-numbered n-alkanes, while the CPI decreases from 4.7 to 3.1. Stable hydrogen isotope values of aquatic alkanes n-C_{23} remain constant (−164 ± 6 ‰), while n-C_{29} increases slightly. Period 2 (23.1–22.5 cal ka BP) is characterized by strongly depleted $\delta D_{n\text{-}C23}$ values (to −450 ‰) and the first appearance of alkane cluster I. Period 3 (22.5–22.0 cal ka BP) is characterized by relatively stable and low concentrations of n-alkanes and mean CPI values of 2.7 ± 0.5. Additionally, $\delta^{15}N$ values decrease for the first time. Period 4 (22.0–21.6 cal ka BP) reveals the lowest concentrations of n-C_{23} and C_{29}. The CPI reaches its maximum at 21.7 cal ka BP because of dominance of odd-numbered n-alkanes, while even-numbered n-alkanes reach minimum concentrations. From this period onward $\delta D_{n\text{-}C29}$ values generally decrease, while $\delta D_{n\text{-}C23}$ starts to fluctuate around its mean value, as it did in Period 1. Furthermore, $\delta^{15}N$ values start to decrease, while $\delta^{13}C$ values increase slightly. During Period 5 (21.6–21.4 cal ka BP), the amount of even-numbered n-alkanes increases rapidly, leading to the lowest CPI values. Period 6 (21.4–21.1 cal ka BP) displays the highest concentrations of odd-numbered n-alkanes, especially n-C_{23}. Until the end of Period 7 (21.1–20.9 cal ka BP), the CPI ranges around 2.4, while the amount of n-alkanes decreases slightly. Additionally, the terrestrial $\delta D_{n\text{-}C29}$ signal shows a shift back to enriched values. Cluster II, representing the aquatic signal, mainly dominates during Periods 3, 4, 6 and 7, whereas cluster III, reflecting the terrestrial signal, stands out during Periods 1–4, and cluster I (microbial signal) dominates during Period 5.

Discussion

$\delta^{13}C_{org}$, $\delta^{15}N$, TOC and TN

$\delta^{13}C_{org}$ values of terrestrial C_3 plants typically range around −28 ‰, whereas those of C_4 plants are clearly higher, ~−14 ‰ (Oleary 1981). Hence, relatively low $\delta^{13}C_{org}$ values of organic matter in the Nam Co sediment samples (−26 ± 1 ‰) may reflect a predominance of C_3 plant material during the LGM. Similar values (−22 to −26 ‰) are documented throughout the Holocene at Nam Co (Mügler et al. 2010), indicating no major change in plant source material since the LGM. Recent palynological and botanical studies also defined this high-alpine region as C_3-dominated, with *Kobresia schoenoides*, *K. pygmaea*, *Morina*, *Oxytropis*, *Stipa*, *Artemisia* and *Poa* (Mügler et al. 2008; Herrmann et al. 2010). However, as lacustrine algae and aquatic macrophytes (emergent, submerged) also use the C_3 pathway, with $\delta^{13}C_{org}$ values ranging between −26 and −6 ‰ (Aichner et al. 2010b), $\delta^{13}C_{org}$ alone should not be used to distinguish between terrestrial and aquatic C_3 plants. A combined interpretation with the TOC/TN ratio, which is independent of the photosynthetic pathway, can generally be used to better assess the source of organic matter (Meyers and Lallier-Verges 1999). Some considerations, however, reduce the potential benefit of these proxies for detailed paleoenvironmental reconstruction: (1) because of rather constant and low TN values during the LGM, the TOC/TN ratio is mainly driven by TOC shifts, which diminish the applicability of TOC/TN ratio for these sediments, (2) $\delta^{13}C_{org}$ and TOC/TN ratios of aquatic macrophytes from Nam Co and other Tibetan lakes (Aichner et al. 2010b) reveal a broader range and higher values, making it hard to detect terrestrial signals if the macrophyte contribution is high. Nevertheless, the influence of aquatic material in Nam Co is (a) highly diverse under high abundance of these sources and (b) confirmed by the n-alkane signature. As the LGM sediments of Nam Co are largely characterized by TOC/TN ratios <10, sedimentary organic matter was apparently produced mainly by algae and macrophytes, but in certain periods also by terrestrial material like soil, as suggested by the alkane distribution. The decline in $\delta^{13}C_{org}$ values at 22.0 cal ka BP potentially reflects a response to lower salinity from increased precipitation (see $\delta D_{n\text{-}C29}$ discussion), whereas the following trend back to higher $\delta^{13}C_{org}$ values was likely caused by increased productivity of submerged macrophytes (Aichner et al. 2010c) as a consequence of higher nutrient supply from glacial meltwater and precipitation input (Slemmons et al. 2013) (see discussion of n-C_{23} amount).

Further paleoenvironmental information can be derived from trends in the stable nitrogen isotopic composition as an indicator of ecosystem regeneration (Rothe and Gleixner 2000). Because the mean $\delta^{15}N$ value of 8 ± 0.4 ‰ in the oldest Nam Co sediments, until 22.5 cal ka BP (Periods 1 and 2), is higher than values in recent organic material, this may indicate a relatively unproductive ecosystem that used mainly old, recycled nitrogen. The $\delta^{15}N$ values in subsequent periods, however, show a decreasing trend, suggesting a more abundant nitrogen supply by nitrogen fixation, as the lake system started to regenerate under the influence of both terrestrial and aquatic organic matter. Furthermore, the amount of TN reflects the trophic status of the aquatic system. Lower temperatures can decrease the decomposition rate and therefore reduce the deposition of TN within the system. At Nam Co the amount of TN is stable, with a mean value of 0.05 ± 0.003 %, i.e. very low variability compared to the Holocene (~0.2 %) (Doberschütz et al. 2014), indicating general reduced productivity and decomposition rates and therefore low deposition of nitrogen in organic matter during the LGM.

Sources and composition of sedimentary *n*-alkanes

In general, the distribution and total amount of *n*-alkanes in lake sediments is an indicator of productivity and/or the level of degradation in a lake system or its catchment, enabling the determination of the relative contributions of autochthonous and allochthonous organic matter (Eglinton and Hamilton 1967; Gelpi et al. 1970; Grimalt and Albaiges 1987; Ficken et al. 2000). These measures can be used to reconstruct relative temperature and precipitation (Lin et al. 2008), although large lakes like Nam Co are assumed to react rather slowly to climate change. The main factors that influence the productivity of aquatic plants are temperature, sunlight intensity, nutrient supply and the availability of dissolved inorganic carbon (Lin et al. 2008). The dominant aquatic *n*-alkane *n*-C_{23} in recent samples, as well as within the older sediments of Nam Co, can be used as a proxy for lake water conditions (Günther et al. 2013). The total amount of *n*-alkanes in the Nam Co sediments between 23.7 and 20.9 cal ka BP is lower (900 ± 360 ng g^{-1}) than in surface sediments (3–28 μg g^{-1}) and during the late Holocene (7–28 μg g^{-1}) (Günther et al. 2011), indicating lower biomass production because of colder and dryer climate conditions during the LGM. Despite low biomass production, the distribution of short-, mid- and long-chain even- and odd-numbered *n*-alkanes enables one to distinguish changes in vegetation type and source.

To identify the sources of short-, mid- and long-chain *n*-alkanes, investigations of different organic materials from the lake and its catchment are necessary. As shown by Eglinton and Hamilton (1967), terrestrial vascular plants preferentially synthesize odd-numbered long-chain *n*-alkanes *n*-$C_{27–33}$, which is confirmed by the *n*-alkane composition of plant samples from the Nam Co catchment (ESM Fig. 2). Although *n*-C_{29} has previously been interpreted as an indicator for tree vegetation (Schwark et al. 2002), it probably represents herbaceous terrestrial vegetation at Nam Co because it is found mainly in alpine meadows and steppe grasses that dominate the local, treeless vegetation. A distinction between the signal of woody and herbaceous plants is not possible because of mixing of different organic matter sources within the lake sediment (Rao et al. 2011). On the other hand, *n*-C_{29} was also found in higher proportions in emergent macrophyte species *Hippuris* and lower abundances in submerged plants (*Potamogeton*, *Batrachium*), with more affinity to shallow lakes that experience dryer conditions (Ficken et al. 2000; Aichner et al. 2010a).

After grazing and subsequent digestion by herbivores, the plant *n*-alkane distribution is mainly unaffected with respect to dominance of *n*-C_{29} and *n*-C_{31}. That is, following the nutrition cycle, digested material is retained in the soil where the same *n*-alkane signature prevails. The input of terrestrial material into the sediment is mainly influenced by the degree of grazing, which entails mobilization of plant material, as well as the strength of aeolian and fluvial transport. Zhao et al. (2003) characterized dust input as the major mechanism transporting terrestrial *n*-alkanes into a lake system. This aeolian transport is assumed to have been stronger in glacial times than during warm and humid periods. In contrast, mid-chain-length, odd-numbered *n*-alkanes *n*-$C_{21–25}$ are mainly produced by submerged and floating aquatic plants (Ficken et al. 2000; Aichner et al. 2010a), which is also confirmed by analyses of aquatic plants from Nam Co (ESM Fig. 2). Gao et al. (2011) showed that up to 97 % of the mid-chain-length *n*-alkane C_{23} in sediments is derived from floating and submerged macrophytes. Furthermore, photosynthetic bacteria and algae synthesize mainly short-chain-length, odd-numbered *n*-alkanes *n*-$C_{15–19}$, with a dominance at *n*-C_{17} (Gelpi et al. 1970). In addition, some microorganisms produce even-numbered *n*-alkanes *n*-$C_{12–22}$ (Grimalt and Albaiges 1987), consistent with analyses of POM from Nam Co (ESM Fig. 2) and reflecting a mixture of mid-chain-length *n*-alkanes from aquatic plants and short-chain-length *n*-alkanes *n*-$C_{17–21}$ derived from algae and/or microbes.

With the incorporation of allochthonous organic material from the catchment into lake sediments, the *n*-alkane composition can be altered in two directions. Whereas fresh, undegraded plant material is characterized by a high odd/even preference of *n*-alkanes and consequently high CPI values (cluster III, ESM Fig. 4), organic matter degraded by soil microorganisms reveals a very low odd/even preference and no chain-length preference (Zech et al. 2011). As a consequence, high input of microbially degraded soil organic matter decreases the sediment CPI (cluster I), whereas intermediate CPI values (cluster II) are characteristic of mainly aquatic-plant-derived organic matter. In general, the sediment organic matter composition of the investigated core section is more strongly influenced by short- to mid-chain *n*-alkanes compared to long-chain *n*-alkanes, resulting in closer similarity to the aquatic and POM signal compared to the terrestrial signal (ESM Fig. 3). Regarding the uncertainty caused by mixing processes from heterogenous organic matter sources, additional information about past changes in the ecosystem can be gleaned from the compound-specific stable hydrogen composition.

Hydrogen source for sedimentary *n*-alkanes

The δD composition of *n*-alkanes from Tibetan lake sediments has recently been shown to provide information about biological sources (Duan et al. 2011) and past environmental and hydrological changes (Mügler et al. 2010; Günther et al. 2011). This is related to the fact that *n*-alkane-synthesizing organisms utilize the ambient water as the primary hydrogen source. Hence, aquatic organisms and macrophytes use the lake water, whereas terrestrial plants mainly utilize meteoric water. Previous studies revealed that the isotopic composition of the lake water, which is reflected by the δD of the aquatic mid-chain *n*-alkane *n*-C_{23}, is modified by evaporation (Günther et al. 2013), whereas the isotopic composition of the precipitation/inflow, reflected by the δD of the terrestrial long-chain *n*-alkane *n*-C_{29}, is modified by meteorological conditions like evapotranspiration and relative moisture (Mügler et al. 2008; Xia et al. 2008; Hu et al. 2014). As a consequence, $\delta D_{n\text{–}C23}$ and $\delta D_{n\text{–}C29}$ can be used as proxies for aquatic and terrestrial hydrological changes, as well as for investigating lake–level changes (Mügler et al. 2008, 2010). Furthermore, comparison of the terrestrial and aquatic δD values can be used to distinguish between large-scale precipitation changes and inflow events. In the case of Nam Co, it has been shown that depleted $\delta D_{n\text{–}C29}$ values are assumed to reflect the greater influence of monsoonal rainfall, whereas enriched $\delta D_{n\text{–}C29}$ values reflect the increased influence of continental moisture sources (e.g. Westerlies) or convective precipitation after evaporation from the lake itself (Mügler et al. 2010). The trend to depleted $\delta D_{n\text{–}C29}$ values starting at ~22 cal ka BP could therefore be interpreted as a general change to wetter conditions resulting in decreased evapotranspiration. In contrast, depleted $\delta D_{n\text{–}C23}$ values may reflect the input of isotopically depleted water (e.g. meltwater from winter snowfall), whereas enriched $\delta D_{n\text{–}C23}$ values likely indicate increased evaporation during summer. Considering this, the strong depletion within Period 2 (23.1–22.5 cal ka BP) could point to initial lake filling by meltwater during the LGM, while $\delta D_{n\text{–}C29}$ data are missing as an indicator for still under-represented terrestrial vegetation. As a consequence, compound–specific δD values of the different *n*-alkanes can be used to differentiate between freshwater input from meltwater and precipitation. Throughout the LGM part of the Nam Co sediment record, the aquatic *n*-C_{23} is more enriched in deuterium than is terrestrial *n*-C_{29}. This is typical for closed lakes under arid conditions that have a negative water balance (Mügler et al. 2008).

Local paleoenvironmental reconstruction

Period 1 (23.7–23.1 cal ka BP)

The first period of the investigated sequence is characterized by large fluctuations in the amount of odd-numbered *n*-alkanes, probably caused by high sensitivity of the small and shallow lake to changes in nutrient supply (Kasper et al. 2015). According to the dominant terrestrial cluster III, lake sediment was almost exclusively influenced by fresh material from macrophytes (emergent, submerged) as well as soil/dung (mainly n-C_{31}). Slight changes in temperature and water supply would have resulted in a larger response of a shallow lake under glacial conditions. The slight increase in TOC and TN, in conjunction with a fairly stable TOC/TN ratio, implies increased decomposition and thus enhanced accumulation of nitrogen within the organic matter caused by periodically warmer conditions. These changes in temperature are also supported by slightly decreased $\delta D_{n\text{–}C29}$ values, but did not influence the lake water isotopic signal to a great extent, as inferred from relatively stable $\delta D_{n\text{–}C23}$ values, as Nam Co had not yet begun to behave like a typical lake.

Period 2 (23.1–22.5 cal ka BP)

This period shows a pronounced lake response to climate changes. A remarkable drop in $\delta D_{n\text{–}C23}$ to strongly depleted values suggests high input of meltwater from the neighbouring Nyainqentanglha Mountain Range at an early stage of deglaciation, when Lake Nam Co was still very small and shallow. If winter precipitation had increased, a thick and long-lasting snow cover would have suppressed the otherwise sparse terrestrial vegetation, and even meltwater during summer could not have provided enough moisture to support n-$C_{29/31}$ biosynthesis. As a consequence, because of the low amount of the terrestrial biomarker, no detailed isotopic information on terrestrial hydrologic conditions could be gathered for this time interval and beyond. The first occurrence of alkane cluster I supports the appearance of periodic, small erosion events limited to meltwater streams.

Period 3 (22.5–22.0 cal ka BP)

After the lake experienced its first main freshwater pulse, the climate situation in Period 3 shifted to the driest and coldest conditions within the investigated interval. Limited production of organic matter as a result of cold climate conditions is also reflected by low amounts of n-alkanes in the sediments, inhibiting the reliable determination of the δD of aquatic and terrestrial biomarkers for most of this period. The pronounced reduction of terrestrial organic matter input via lowered erosion and/or productivity is inferred from the absence of C_{31} n-alkanes. The major input was derived from aquatic organisms, as reflected by cluster II. Persistent low TOC/TN ratios and decreased $\delta^{15}N$ values point to a further dominance of aquatic organic matter, likely from emergent macrophytes. Decreasing amounts of TOC and TN, however, may reflect reduced within-lake productivity and reduced deposition of organic matter may have beeen a consequence of climate cooling.

Period 4 (22.0–21.6 cal ka BP)

During Period 4, the trend toward higher TOC content and therefore higher TOC/TN ratios, as well as decreased $\delta^{13}C_{org}$ and $\delta^{15}N$ values, indicates enhanced input of terrestrial organic material. Additionally, lowest amounts of even-numbered n-alkanes and consequent maximum CPI values suggest the input of fresh material. This increased input is probably related to higher rates of precipitation, indicated by the trend toward depleted $\delta D_{n\text{–}C29}$ values beginning at 22.0 cal ka BP. Changes in the lake water isotopic signal ($\delta D_{n\text{–}C23}$) are not significant, reflecting an attenuated lake response. There is an apparent inconsistency between increasing TOC content and the decreasing amount of n-alkanes. Nevertheless, lowest amounts of n-C_{23} and of n-C_{29} indicate cold conditions, which should have reduced productivity in the lake and catchment.

Period 5 (21.6–21.4 cal ka BP)

Period 5 is characterized by the highest amounts of even-numbered n-alkanes as well as high n-C_{31} input, originating from degraded soil and dung organic matter. The large contribution of reworked material lowers the CPI value to ~ 1 (cluster I). Low CPI values are in accordance with decreasing $\delta^{15}N$ values, reflecting a continuously rising supply of terrestrial organic matter to the lake. This likely reflects erosional processes in the catchment, probably triggered by enhanced runoff from increased precipitation and/or melting glaciers. The $\delta D_{n\text{–}C23}$ values fluctuate around the mean and $\delta D_{n\text{–}C29}$ values continue to decrease, suggesting enhanced precipitation, which generated erosion events under warmer and wetter conditions starting at 21.6 cal ka BP, in agreement with increased input of microbially degraded soil material. Because terrestrial vegetation was not yet fully developed, unimpeded precipitation eroded soil material, which is evident in increased sediment accumulation rates (Fig. 3l).

Period 6 (21.4–21.0 cal ka BP)

Significant environmental change initiated during Period 5 carried on into Period 6, reflected by the rising amount of aquatic n-C_{23}. This strong increase in biomass production of mainly aquatic macrophytes (n-C_{23}), likely induced by enhanced water-column mixing and nutrient supply from freshwater input (Slemmons et al. 2013), is supported by rather low $\delta D_{n\text{–}C23}$ values and very high $\delta^{13}C$ values. Higher $\delta D_{n\text{–}C29}$ values are indicative of reduced precipitation. Consequently, the low $\delta D_{n\text{–}C23}$ values are likely related to inflow of glacial meltwater rather than input of isotopically light rainwater. Additionally, input by terrestrial n-C_{31} decreased to the point of absence in some samples.

Period 7 (21.0–20.9 cal ka BP)

High variability in almost all climate proxies suggests a system with pronounced climate fluctuations during brief Period 7. $\delta^{13}C_{org}$ and TOC reached maximum values whereas $\delta^{15}N$ reached minimum values at 20.9 cal ka BP. This may indicate high within-lake biomass productivity dominating the contribution to sedimentary organic matter, a result of high nutrient availability from additional input of allochthonous organic material. Thus, this period can be characterized by climate conditions similar to those of Period 1. In addition, high $\delta D_{n\text{–}C29}$ values also suggest a shift back to arid conditions, i.e. decreased amounts of precipitation.

Although the onset of mountain glacier retreat on the Tibetan Plateau is generally believed to have occurred only between 18 and 16 cal ka BP, our results indicate that first retreat events likely occurred by 23 cal ka BP in the Nam Co region. This might be related to increasing temperatures, which most likely affected glaciers in the Nyainqentanglha Mountain Range south of Nam Co. Meltwater runoff was probably confined to river channels, as the input of reworked soil organic matter was rather limited, illustrated by moderate CPI values. Because the catchment vegetation was not fully developed, precipitation influenced sediment accumulation rates to a greater extent during the LGM. Changing climate conditions, i.e. temperature and precipitation fluctuations, are reflected in cyclic variations of n-alkane amounts during this interval, and initiated the gradual formation of a larger lake.

Regional paleoclimate

The Nam Co sediment record can be compared with relevant paleoclimate records like the Greenland ice cores, Hulu Cave stalagmites (east China), Lake Qinghai sediments (northern Tibetan Plateau) and East Arabian Sea sediments, to reveal connections between regional climate evolution on the Tibetan Plateau and changes elsewhere in the northern hemisphere (Fig. 4). The primary driving force for long-term climate variations was the amount of orbitally forced solar irradiation, which influenced global atmospheric circulation. The main driving air mass at Nam Co during the LGM, and also the one responsible for abrupt climate changes on the northern Tibetan Plateau (e.g. Lake Qinghai), was the mid-latitude Westerlies wind system, which is directly controlled by Atlantic meridonal overturning circulation (Sun et al. 2012).

Changes in atmospheric circulation on centennial to millennial time scales, however, are not explained by solar irradiation changes (Yao et al. 2001). Two such abrupt circulation changes during the LGM caused the cold Heinrich-2 event (H-2) and the subsequent warm Greenland Interstadial 2 (GI-2) (Fig. 4). The cold/dry and dust–rich H-2 event is recorded between 24.3 and 23.5 cal ka BP in the NGRIP, GRIP and GISP2 Greenland ice core records (Rasmussen et al. 2008), in Hulu Cave between 24.4 and 23.6 cal ka BP (Wang et al. 2001), in Lake Qinghai sediments between 24.1 and 23.5 cal ka BP (An et al. 2012) and in the East Arabian Sea Surface Temperature (SST) record between 24.2 and 23.3 cal ka BP (Mahesh and Banakar 2014). This indicates an intra-hemispheric coupling of climate events in Greenland and Asia, which can be explained by intensified Westerlies, a consequence of a cold and ice-covered North Atlantic Ocean (An et al. 2012). It is possible that at ~23.5 cal ka BP, shallow Nam Co, which was characterized by dramatic stage fluctuations (Period 1), was influenced by the cold and dry H-2 event. However, because general climate conditions at shallow Nam Co during that time were already dry and cold, evidence from compound-specific data do

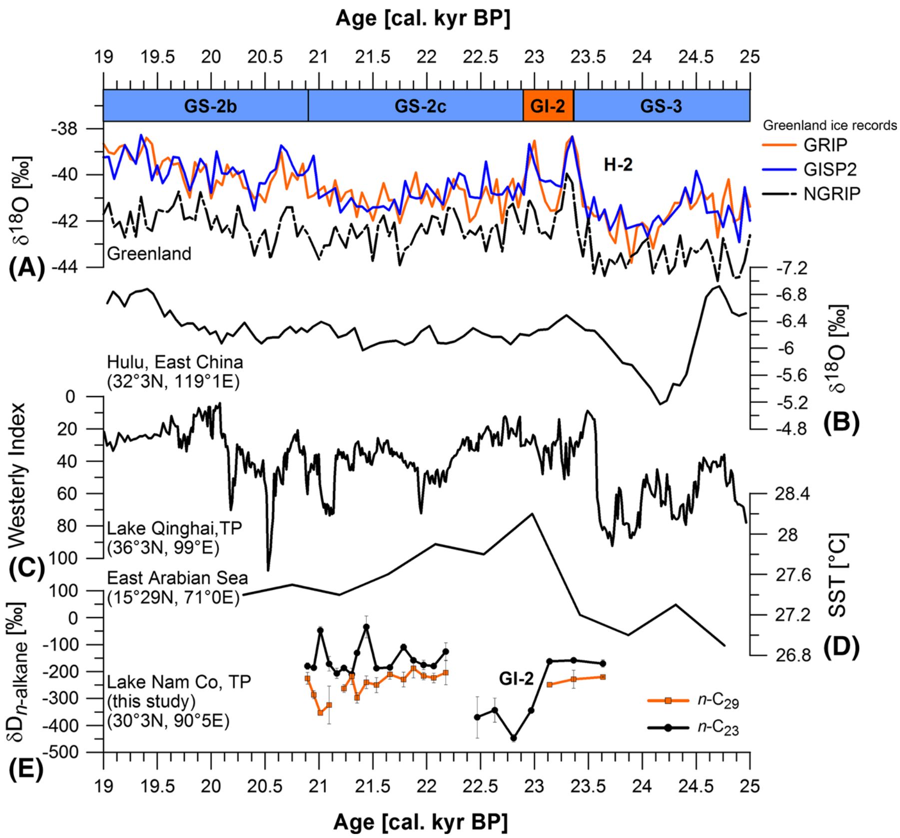

Fig. 4 Comparison of proxy records from different locations between 25 and 19 cal ka BP. Greenland Stadials (GS-2b, GS-2c) and Greenland Interstadial 2 (GI-2), following Lowe et al. (2008). The Heinrich-2 event (H-2) is marked, following Moreno et al. (2010). **a** $\delta^{18}O$ from three Greenland ice cores, as in Rasmussen et al. (2008): GRIP (Johnsen et al. 1997), GISP2 (Stuiver and Grootes 2000) and NGRIP (Andersen et al. 2004), **b** $\delta^{18}O$ of stalagmites from Hulu Cave, eastern China (Wang et al. 2001), **c** lake Qinghai Westerlies climate index from flux of >25 µm sediment fraction (An et al. 2012), **d** sea surface temperature calculated from Mg/Ca ratios of the planktic foraminifer *G. sacculifer* in the East Arabian Sea (Mahesh and Banakar 2014), **e** δD_{n-C23} and δD_{n-C29} of ***n***-alkanes in sediment core NC 08/01 from Nam Co, south-central Tibet (this study)

not support the H-2 onset. The subsequent warmer GI-2 is also visible in the other records, starting at 23.5 ± 0.2 cal ka BP. During Period 2, a significant response is indicated by low δD_{n-C23} values, indicating increased meltwater input from warmer conditions. The impact of the warmer GI-2 event was less severe on the sparse catchment vegetation, perhaps because the thawing season was too short, providing insufficient time for vegetation regeneration.

Previous studies (Yao et al. 1997) suggested that the Tibetan Plateau, and hence the Nam Co region, reacts more sensitively to climate change than does Greenland. A second freshwater period was detected at Nam Co, starting at 22.0 cal ka BP, in the middle of the colder Greenland Stadial 2c event (GS-2c), which is in general agreement with the GISP2 and GRIP records. After reaching a certain threshold of energy in the system, the precipitation amount or temperature affects the input of nutrients and/or melting. Thus, Nam Co went through several developmental stages from glacial conditions to a deglaciation stage. The freshwater periods at Nam Co could have been precursors for the onset or strengthening of the IOSM during the LGM. Abruptly increasing temperatures would have reduced snow cover on the Tibetan Plateau and therefore increased surface temperature and radiative heating. Consequently, if warming of the Indian Ocean was synchronous with the deglaciation of continental ice sheets, the abrupt freshwater event at Nam Co could be a sign of an early deglaciation pulse on the southern Tibetan Plateau, probably forced by weakening of the winter monsoon and a stronger summer monsoon.

Conclusions

The sediment record from Nam Co, south-central Tibetan Plateau, reflects the early stages of deglaciation during the LGM in a climate-sensitive high-altitude region. Evidence for two distinct freshwater periods was found using stable hydrogen isotope composition, *n*-alkane distribution and concentration, as well as bulk sediment TOC, TN, $\delta^{13}C_{org}$ and $\delta^{15}N$ composition in sediments deposited between 23.7 and 20.9 cal ka BP. Lake system and catchment development, as responses to intra-hemispheric climate events, were described for seven periods at Nam Co. This study also aimed to determine whether Nam Co was continuously ice-covered during the LGM, and, if not, what factors provided thawing energy. Compared to the Holocene, colder and dryer conditions during the LGM strongly suppressed terrestrial vegetation. Periodic erosion events led to highest sediment accumulation rates until growth of vegetation prevented excessive erosion to shallow Nam Co. The majority of organic matter was produced by aquatic organisms, recording the isotopic signal of lake water. Coldest conditions are inferred for the interval between 22.5 and 22.0 cal ka BP. However, even during that period, ice cover was temporarily interrupted by short thaw periods during summer. High amounts of even-numbered *n*-alkanes indicate increased erosional input of soil material into the lake between 21.6 and 21.4 cal ka BP. More obvious environmental changes occurred after 23.1 cal ka BP, with the influence of the warmer Greenland Interstadial-2 event leading to very low $\delta D_{n\text{–}C23}$ values, while $\delta D_{n\text{–}C29}$ values remained rather high. This likely indicates meltwater inflow from the Nyainqentanglha Mountain Range. A second freshwater period, induced by increased precipitation, was detected by changes in *n*-alkane distribution and depleted terrestrial $\delta D_{n\text{–}C29}$ values starting at 22.0 cal ka BP. This period is characterized by several deglacial developmental stages in the middle of the colder Greenland Stadial 2c event. On millennial timescales, environmental changes were caused by a slightly intensified IOSM and attenuated Westerlies during winter. Apparently, the first evidence for deglaciation at Nam Co was preceded by at least two earlier glacier-melting phases between 23.1 and 21.1 cal ka BP, within the warmer Greenland Interstadial 2 and colder Greenland Stadial 2c events.

Acknowledgments We thank Steffen Rühlow and Heike Geilmann (MPI–BGC, Jena) for help with δD and bulk sediment isotopic measurements and Birgit Plessen (GFZ, Potsdam) for bulk isotopic measurements on catchment samples. We also thank the working group from the Institute of Geography, Friedrich Schiller University Jena for their support, and our Chinese colleagues Zhu Liping and Wang Junbo for their help during field work. This work was performed in joint cooperation with the Institute of Tibetan Plateau Research and funded by the German Research Foundation (DFG Grant Gl262/15).

References

Aichner B, Herzschuh U, Wilkes H (2010a) Influence of aquatic macrophytes on the stable carbon isotopic signatures of sedimentary organic matter in lakes on the Tibetan Plateau. Org Geochem 41:706–718

Aichner B, Herzschuh U, Wilkes H, Vieth A, Bohner J (2010b) δD values of n-alkanes in Tibetan lake sediments and aquatic macrophytes—a surface sediment study and application to a 16 ka record from Lake Koucha. Org Geochem 41:779–790

Aichner B, Wilkes H, Herzschuh U, Mischke S, Zhang CJ (2010c) Biomarker and compound-specific delta C-13 evidence for changing environmental conditions and carbon limitation at Lake Koucha, eastern Tibetan Plateau. J Paleolimnol 43:873–899

An ZS, Colman SM, Zhou WJ, Li XQ, Brown ET, Jull AJT, Cai YJ, Huang YS, Lu XF, Chang H, Song YG, Sun YB, Xu H, Liu WG, Jin ZD, Liu XD, Cheng P, Liu Y, Ai L, Li XZ, Liu XJ, Yan LB, Shi ZG, Wang XL, Wu F, Qiang XK, Dong JB, Lu F, Xu XW (2012) Interplay between the Westerlies and Asian monsoon recorded in Lake Qinghai sediments since 32 ka. Sci Rep 2:619

Andersen KK, Azuma N, Barnola JM, Bigler M, Biscaye P, Caillon N, Chappellaz J, Clausen HB, DahlJensen D, Fischer H, Fluckiger J, Fritzsche D, Fujii Y, Goto-Azuma K, Gronvold K, Gundestrup NS, Hansson M, Huber C, Hvidberg CS, Johnsen SJ, Jonsell U, Jouzel J, Kipfstuhl S, Landais A, Leuenberger M, Lorrain R, Masson-Delmotte V, Miller H, Motoyama H, Narita H, Popp T, Rasmussen SO, Raynaud D, Rothlisberger R, Ruth U, Samyn D, Schwander J, Shoji H, Siggard-Andersen ML, Steffensen JP, Stocker T, Sveinbjornsdottir AE, Svensson A, Takata M, Tison JL, Thorsteinsson T, Watanabe O, Wilhelms F, White JWC, Project NGIC (2004) High-resolution record of Northern Hemisphere climate extending into the last interglacial period. Nature 431:147–151

Barrows TT, Juggins S (2005) Sea-surface temperatures around the Australian margin and Indian ocean during the last glacial maximum. Quat Sci Rev 24:1017–1047

Bolch T, Yao T, Kang S, Buchroithner MF, Scherer D, Maussion F, Huintjes E, Schneider C (2010) A glacier inventory for the western Nyainqentanglha Range and the Nam Co Basin, Tibet, and glacier changes 1976-2009. Cryosphere 4:419–433

Chabangborn A, Brandefelt J, Wohlfarth B (2014) Asian monsoon climate during the last glacial maximum: palaeo-data-model comparisons. Boreas 43:220–242

Chen B, Xu XD, Yang S, Zhang W (2012) On the origin and destination of atmospheric moisture and air mass over the Tibetan Plateau. Theor Appl Climatol 110:423–435

Clark PU, Dyke AS, Shakun JD, Carlson AE, Clark J, Wohlfarth B, Mitrovica JX, Hostetler SW, McCabe AM (2009) The last glacial maximum. Science 325:710–714

Daut G, Mäusbacher R, Baade J, Gleixner G, Kroemer E, Mügler I, Wallner J, Wang J, Zhu L (2010) Late quaternary hydrological changes inferred from lake level fluctuations of Nam Co (Tibetan Plateau, China). Quat Int 218:86–93

Doberschütz S, Frenzel P, Haberzettl T, Kasper T, Wang J, Zhu L, Daut G, Schwalb A, Mäusbacher R (2014) Monsoonal forcing of Holocene paleoenvironmental change on the central Tibetan Plateau inferred using a sediment record from Lake Nam Co (Xizang, China). J Paleolimnol 51:253–266

Duan Y, Wu BX, Xu L, He JX, Sun T (2011) Characterisation of n-alkanes and their hydrogen isotopic composition in sediments from Lake Qinghai, China. Org Geochem 42:720–726

Eglinton G, Hamilton RJ (1967) Leaf epicuticular waxes. Science 156:1322

Ficken KJ, Li B, Swain DL, Eglinton G (2000) An n-alkane proxy for the sedimentary input of submerged/floating freshwater aquatic macrophytes. Org Geochem 31: 745–749

Gao L, Hou JZ, Toney J, MacDonald D, Huang Y (2011) Mathematical modeling of the aquatic macrophyte inputs of mid-chain n-alkyl lipids to lake sediments: implications for interpreting compound specific hydrogen isotopic records. Geochim Cosmochim Acta 75:3781–3791

Gelpi E, Schneide H, Mann J, Oro J (1970) Lipids of geochemical significance in microscopic algae. 1. Hydrocarbons of geochemical significance in microscopic algae. Phytochemistry 9:603

Grimalt J, Albaiges J (1987) Sources and occurence of C-12-C22 normal-alkane distributions with even carbon-number preference in sedimentary environments. Geochim Cosmochim Acta 51:1379–1384

Günther F, Mügler I, Mäusbacher R, Daut G, Leopold K, Gerstmann UC, Xu B, Yao T, Gleixner G (2011) Response of delta D values of sedimentary n-alkanes to variations in source water isotope signals and climate proxies at lake Nam Co, Tibetan Plateau. Quat Int 236:82–90

Günther F, Aichner B, Siegwolf R, Xu B, Yao T, Gleixner G (2013) A synthesis of hydrogen isotope variability and its hydrological significance at the Qinghai–Tibetan Plateau. Quat Int 313:3–16

Günther F, Witt R, Schouten S, Mäusbacher R, Daut G, Zhu L, Xu B, Yao T, Gleixner G (2015) Quaternary ecological responses and impact of the Indian Ocean Summer Monsoon at Nam Co, Southern Tibetan Plateau. Quat Sci Rev 112:66–77

Herrmann M, Lu XM, Berking J, Schütt B, Yao TD, Mosbrugger V (2010) Reconstructing Holocene vegetation and climate history of Nam Co area (Tibet), using pollen and other palynomorphs. Quat Int 218:45–57

Hou J, D'Andrea WJ, Liu Z (2012) The influence of 14C reservoir age on interpretation of paleolimnological records from the Tibetan Plateau. Quat Sci Rev 48:67–79

Hu X, Zhu L, Wang Y, Wang J, Peng P, Ma Q, Hu J, Lin X (2014) Climatic significance of n-alkanes and their compound-specific delta D values from lake surface sediments on the Southwestern Tibetan Plateau. Chin Sci Bull 59:3022–3033

Hughes PDG, Gibbard PL, Ehlers J (2013) Timing of glaciation during the last glacial cycle: evaluating the concept of a global 'Last Glacial Maximum'. Earth Sci Rev 125: 171–198

Johnsen SJ, Clausen HB, Dansgaard W, Gundestrup NS, Hammer CU, Andersen U, Andersen KK, Hvidberg CS, DahlJensen D, Steffensen JP, Shoji H, Sveinbjornsdottir AE, White J, Jouzel J, Fisher D (1997) The delta O-18 record along the Greenland Ice Core Project deep ice core and the problem of possible Eemian climatic instability. J Geophys Res Oceans 102:26397–26410

Kasper T, Haberzettl T, Wang J, Daut G, Zhu L, Mäusbacher R (2015) Hydrological variations on the Central Tibetan Plateau since the Last Glacial Maximum and their teleconnection to inter-regional and hemispheric climate variations. J Quat Sci 30:70–78

Lambeck K, Yokoyama Y, Purcell T (2002) Into and out of the Last Glacial Maximum: sea-level change during Oxygen Isotope Stages 3 and 2. Quat Sci Rev 21:343–360

Li MH, Kang SC, Zhu LP, You QL, Zhang QG, Wang JB (2008) Mineralogy and geochemistry of the Holocene lacustrine sediments in Nam Co, Tibet. Quat Int 187:105–116

Lin X, Zhu L, Wang Y, Wang J, Xie M, Ju J, Mäubacher R, Schwalb A (2008) Environmental changes reflected by n-alkanes of lake core in Nam Co on the Tibetan Plateau since 8.4 kaBP. Chin Sci Bull 53:3051–3057

Liu J, Kang S, Gong T, Lu A (2010) Growth of a high-elevation large inland lake, associated with climate change and permafrost degradation in Tibet. Hydrol Earth Syst Sci 14:481–489

Lowe JJ, Rasmussen SO, Bjorck S, Hoek WZ, Steffensen JP, Walker MJC, Yu ZC, Grp I (2008) Synchronisation of palaeoenvironmental events in the North Atlantic region during the Last Termination: a revised protocol recommended by the INTIMATE group. Quat Sci Rev 27:6–17

Mahesh BS, Banakar VK (2014) Change in the intensity of low-salinity water inflow from the Bay of Bengal into the Eastern Arabian Sea from the Last Glacial Maximum to the Holocene: implications for monsoon variations. Palaeogeogr Palaeoclimatol Palaeoecol 397:31–37

Meyers PA, Lallier-Verges E (1999) Lacustrine sedimentary organic matter records of Late Quaternary paleoclimates. J Paleolimnol 21:345–372

Mix AC, Bard E, Schneider R (2001) Environmental processes of the ice age: land, oceans, glaciers (EPILOG). Quat Sci Rev 20:627–657

Moreno A, Stoll H, Jimenez-Sanchez M, Cacho I, Valero-Garces B, Ito E, Edwards RL (2010) A speleothem record of glacial (25–11.6 kyr BP) rapid climatic changes from northern Iberian Peninsula. Global Planet Change 71:218–231

Mügler I, Sachse D, Werner M, Xu BQ, Wu GJ, Yao TD, Gleixner G (2008) Effect of lake evaporation on delta D values of lacustrine n-alkanes: a comparison of Nam Co (Tibetan Plateau) and Holzmaar (Germany). Org Geochem 39:711–729

Mügler I, Gleixner G, Günther F, Mäusbacher R, Daut G, Schütt B, Berking J, Schwalb A, Schwark L, Xu B, Yao T, Zhu L, Yi C (2010) A multi-proxy approach to reconstruct hydrological changes and Holocene climate development of Nam Co, Central Tibet. J Paleolimnol 43:625–648

Oleary MH (1981) Carbon isotope fractionation in plants. Phytochemistry 20:553–567

Polissar PJ, Freeman KH, Rowley DB, McInerney FA, Currie BS (2009) Paleoaltimetry of the Tibetan Plateau from D/H ratios of lipid biomarkers. Earth Planet Sci Lett 287:64–76

Ramsey CB (1995) Radiocarbon calibration and analysis of stratigraphy: the OxCal program. Radiocarbon 37:425–430

Rao ZG, Wu Y, Zhu ZY, Jia GD, Henderson A (2011) Is the maximum carbon number of long-chain n-alkanes an indicator of grassland or forest? Evidence from surface soils and modern plants. Chin Sci Bull 56:1714–1720

Rasmussen SO, Selerstad IK, Andersen KK, Bigler M, Dahl-Jensen D, Johnsen SJ (2008) Synchronization of the NGRIP, GRIP, and GISP2 ice cores across MIS 2 and palaeoclimatic implications. Quat Sci Rev 27:18–28

Rothe J, Gleixner G (2000) Do stable isotopes reflect the food web development in regenerating ecosystems? Isotopes Environ Health Stud 36:285–301

Sachse D, Radke J, Gleixner G (2006) delta D values of individual n-alkanes from terrestrial plants along a climatic gradient—implications for the sedimentary biomarker record. Org Geochem 37:469–483

Schütt B, Berking J, Frechen M, Frenzel P, Schwalb A, Wrozyna C (2010) Late quaternary transition from lacustrine to a fluvio-lacustrine environment in the north-western Nam Co, Tibetan Plateau, China. Quat Int 218:104–117

Schwark L, Zink K, Lechterbeck J (2002) Reconstruction of postglacial to early Holocene vegetation history in terrestrial Central Europe via cuticular lipid biomarkers and pollen records from lake sediments. Geology 30:463–466

Shi Y (2002) Characteristics of late quaternary monsoonal glaciation on the Tibetan Plateau and in East Asia. Quat Int 97–8:79–91

Slemmons KEH, Saros JE, Simon K (2013) The influence of glacial meltwater on alpine aquatic ecosystems: a review. Environ Sci Process Impacts 15:1794–1806

Steinbeiss S, Temperton VM, Gleixner G (2008) Mechanisms of short-term soil carbon storage in experimental grasslands. Soil Biol Biochem 40:2634–2642

Stuiver M, Grootes PM (2000) GISP2 oxygen isotope ratios. Quatern Res 53:277–283

Sun YB, Clemens SC, Morrill C, Lin XP, Wang XL, An ZS (2012) Influence of Atlantic meridional overturning circulation on the East Asian winter monsoon. Nat Geosci 5:46–49

Wang Y, Sessions AL (2008) Memory effects in compound-specific D/H analysis by gas chromatography/pyrolysis/isotope-ratio mass spectrometry. Anal Chem 80:9162–9170

Wang YJ, Cheng H, Edwards RL, An ZS, Wu JY, Shen CC, Dorale JA (2001) A high-resolution absolute-dated Late Pleistocene monsoon record from Hulu Cave, China. Science 294:2345–2348

Wang X, Feng L, Zhang F, Ding Z (2008) On-line measurements of delta N-15 in biological fluids by a modified continuous-flow elemental analyzer with an isotope-ratio mass spectrometer. Rapid Commun Mass Spectrom 22:1196–1202

Wang R, Yang XD, Langdon P, Zhang EL (2011) Limnological responses to warming on the Xizang Plateau, Tibet, over the past 200 years. J Paleolimnol 45:257–271

Werner RA, Brand WA (2001) Referencing strategies and techniques in stable isotope ratio analysis. Rapid Commun Mass Spectrom 15:501–519

Xia ZH, Xu BQ, Mügler I, Wu GJ, Gleixner G, Sachse D, Zhu LP (2008) Hydrogen isotope ratios of terrigenous n-alkanes in lacustrine surface sediment of the Tibetan Plateau record the precipitation signal. Geochem J 42:331–338

Yao TD, Thompson LG, Shi YF, Qin DH, Jiao KQ, Yang ZH, Tian LD, Thompson EM (1997) Climate variation since the last interglaciation recorded in the Guliya ice core. Sci China Ser D Earth Sci 40:662–668

Yao TD, Xu BQ, Pu JC (2001) Climatic changes on orbital and sub-orbital time scale recorded by the Guliya ice core in Tibetan Plateau. Sci China Ser D Earth Sci 44:360–368

Zech M, Pedentchouk N, Buggle B, Leiber K, Kalbitz K, Markovic SB, Glaser B (2011) Effect of leaf litter degradation and seasonality on D/H isotope ratios of n-alkane biomarkers. Geochim Cosmochim Acta 75:4917–4928

Zhao MX, Dupont L, Eglinton G, Teece M (2003) n-alkane and pollen reconstruction of terrestrial climate and vegetation for NW Africa over the last 160 kyr. Org Geochem 34:131–143

Zhou S, Kang S, Chen F, Joswiak DR (2013) Water balance observations reveal significant subsurface water seepage from Lake Nam Co, south-central Tibetan Plateau. J Hydrol 491:89–99

Zhu LP, Xie MP, Wu YH (2010) Quantitative analysis of lake area variations and the influence factors from 1971 to 2004 in the Nam Co basin of the Tibetan Plateau. Chin Sci Bull 55:1294–1303